Tridiagonal Fermi resonance structure in the vibrational spectrum of the CH chromophore in CHF_3. II. Visible spectra

J. Segall and R. N. Zare
Department of Chemistry, Stanford University, Stanford, California 94305
H. R. Dübal, M. Lewerenz, and M. Quack
Laboratorium für Physikalische Chemie der ETH Zürich (Zentrum), CH-8092 Zürich, Switzerland

(Received 5 August 1986; accepted 11 September 1986)

The near IR and visible vibrational absorption spectra of CHF_3 were recorded up to wave numbers of 17 500 cm^{-1} providing complete frequency coverage, together with paper I, from the low frequency fundamentals to the $N = 6$ CH stretching–bending overtone multiplet. All strong bands in the high overtone spectra could be predicted and assigned by means of the tridiagonal Fermi resonance Hamiltonian, including a few combinations with intense CF_3 stretching vibrations already observed for the low overtones. Improved vibrational Fermi resonance constants are presented on the basis of a fit to 35 assigned bands. An analysis of the rotational fine structure of the $2\nu_4$ (E) overtone component and several Fermi resonance component bands result in values for α_b and α_s, which allow us to determine B_e. In the high overtone bands no rotational fine structure is observed. The bands can be understood by introducing additional homogeneous rovibrational structures of phenomenological widths $\Gamma \approx 1$ to 10 cm^{-1}. The results are discussed in relation to the separation of time scales for mode selective vibrational redistribution and further evolution. The overtone band strengths are reported and analyzed approximately with the empirical local Mecke dipole function.

I. INTRODUCTION

As early as 1948 Bernstein and Herzberg had reported the spectrum of CHF_3 in the near infrared and red part of the visible spectrum.[1] They derived an approximate structure for this molecule and identified the regular occurence of a two state Fermi resonance assigned to the stretching (v_s) and bending (v_b) vibrational states of the CH chromophore $|v_s = N, v_b = 0\rangle$; $|v_s = N - 1, v_b = 2\rangle$. As was shown later[2–5] this resonance is really part of a multiplet system with $n = v_s^{\max} + 1 = N + 1$ strongly interacting states with a fundamental effective coupling parameter $k_{sbb} \approx 100$ cm^{-1}. This coupling leads to ultrafast selective subpicosecond redistribution of vibrational energy between stretching and bending motions and it was shown that the interaction with further modes occurs only on much longer time scales,[3] if at all. Work on other molecules containing the isolated CH chromophore showed that the subpicosecond redistribution is a universal property of the alkyl CH chromophore.[6–9]

Only shortly after the original identification of the importance of the CH stretch bend Fermi resonance interaction for vibrational redistribution in hydrocarbons,[2,3] Sibert *et al.*[10] proposed a similar mechanism in order to explain the subpicosecond vibrational redistribution inferred by Bray and Berry[11] from their photoacoustic visible overtone spectra of benzene. As we have discussed before,[7] due to the lack of well defined structure in the benzene overtone spectra, the interpretation must remain ambiguous in this case. However, we have recently shown at least in one case, that a similarly strong resonance definitely *does* occur also on the sp^2 C atom.[12] The resonance seems thus to be of general importance in hydrocarbons (excluding acetylenes[2,13]) and is also of great interest in understanding some fundamental aspects of vibrational redistribution and intramolecular statistical mechanics.[14,15] It is presumably of importance also for the understanding of *inter*molecular energy transfer.[21]

Following the previous, detailed analysis of the CH chromophore spectrum in the infrared, with stretching quantum numbers up to $N = 4$ (Ref. 5, paper I), we have since then measured the complete visible spectrum of CHF_3 from 11 000 up to about 17 500 cm^{-1} in order to test the predictions from the tridiagonal effective Fermi resonance Hamiltonian and in order to answer additional questions concerning the possibility of further homogeneous rovibrational structure at very high excitations[4] [similar, say, to the large molecule $(CF_3)_3CH$ [7]] and also the band strength and dipole function.[16–18] In the course of this work, some additional information on the CHF_3 spectra became available from previous work on photoacoustic spectra,[19] which covered essentially the spectral range of interest here, but incompletely and without adequate assignments of the Fermi resonance. Furthermore, motivated by our own work, Campargue and Stoeckel[20] have measured the $N = 5$ polyad at high resolution using their elegant ICLAS technique (about 0.02 cm^{-1} bandwidth). We also have remeasured improved Fourier transform spectra of the $N = 5$ polyad, thus providing overlap from various techniques for the $N = 4$ and $N = 5$ polyad. There is agreement between the data from different sources, wherever there is overlap. The aim of the present paper is to provide a *complete analysis* of all strong bands in the visible spectrum. We refer to paper I[5] for more complete references to previous work on the CHF_3 spectra and mention that recently the potentially analogous situation in

 0021-9606/87/020634-13$02.10

CDF_3 has been investigated, which turns out to be fundamentally different, however.[18,22]

II. EXPERIMENTAL

CHF_3 was obtained commercially. Its purity and identity was checked by IR spectroscopy and gas chromatrography and it was thoroughly degassed by repeated freeze–pump–thaw cycles before use, particularly so for the measurements of band strengths. Sample pressures were measured with calibrated capacitance manometers.

The Fourier transform spectra were measured on a BOMEM DA002 allowing for a maximum apodized resolution of 0.004 cm^{-1}. In practice the spectra in the visible are limited by pressure broadening to bandwidths of about 0.5 cm^{-1} at best. Details of the technique have been described before.[5] Improved optical filtering allowed us to obtain improved signal to noise for the spectrum of the $N = 5$ polyad around 14 000 cm^{-1}, which has been remeasured completely.

Most of the data in the present paper, from 11 000 to 17 500 cm^{-1}, were obtained using intracavity cw dye laser photoacoustic techniques, which have been described in detail in Refs. 7, 23, and 24. Briefly, a glass cell fitted with quartz windows at Brewster's angle and Knowles BT-1759 microphone is filled with a sample of CHF_3 at pressures between 5 and 13 kPa. Sometimes inert gas was added (up to about 10^5 Pa Ne). The cell is then placed inside the extended cavity of a Spectra Physics 375 dye laser. A variable speed light chopper is used to interrupt periodically the pump beam from an ion laser, and a lock-in amplifier (PAR 124A) monitors the microphone signal modulated at the chopping frequency. The photoacoustic signal is then normalized to the intracavity laser power, which is measured from a reflection off a cell window. In the 2 cm^{-1} resolution scans the tuning of the laser is achieved by using a stepping motor to rotate a 3-plate birefringent filter inside the dye laser. For the 0.2 cm^{-1} resolution scans a thin étalon (Spectra Physics 411-650) is tuned simultaneously with the birefringent filter. A part of the output of the laser is directed to a neon optogalvanic cell, which provided absolute wavelength calibration, while another part of the output beam traveled through a solid étalon (FSR = 17.4 cm^{-1}) to a photodiode, giving a relative frequency scale. The uncertainties in the frequency measurements are mainly given by the resolution of the laser system used. The analog output of the experiments was digitized off line and stored on floppy disk for transfer and further evaluation of the data.

As the photoacoustic technique does not directly provide absorption cross sections, these were determined by comparing the photoacoustic signals from CHF_3 with published values for benzene.[25] In the ranges of the $N = 5$ and $N = 6$ polyads we used mixed gas samples of benzene and neopentane to determine the neopentane peak cross section and then a mix of neopentane and CHF_3 to obtain cross sections for the latter. Neopentane was used because its overtones lie to the red of the CHF_3 absorptions, while the benzene spectra overlap those of CHF_3. A second technique was used in addition. Here spectra of pure benzene and CHF_3 are taken under identical conditions. Assuming ideal gas behavior one should have approximately[26]

$$\frac{\sigma(CHF_3)}{\sigma(\text{benzene})} = \frac{S(CHF_3)\ C_v(CHF_3)}{S(\text{benzene})\ C_v(\text{benzene})}.$$

The S are the photoacoustic signals, the C_v the specific heats, and the σ the absorption cross sections of the corresponding compounds. The intensities of half-integral polyads were determined by employing laser dyes that allowed for tuning over the high frequency bands of the half-integral polyad and the low frequency bands of the next higher integral polyad.

III. RESULTS AND DISCUSSION

A. Survey of the photoacoustic spectra in the visible range

Figure 1 shows the spectrum of CHF_3 from 12 000 to 17 000 cm^{-1}. There is no strong absorption in the small ranges between the various parts, which have all been measured, and beyond 16 800 to 17 500 cm^{-1}. The spectral coverage is thus complete, at least as far as strong absorptions are concerned. The photoacoustic data extend down to 11 000 cm^{-1} but this range is not shown as it agrees well with the FTIR data (Fig. 7 of Ref. 5), the latter being somewhat more accurate. The absolute cross sections on the ordinate have been computed from the integrated band strengths and the maxima are only approximate due to the 2 cm^{-1} bandwidth in these scans (see Sec. III F). Each part of the survey spectrum corresponds to one polyad, the expected multiplet structure being nicely exhibited as in the IR spectra of CHF_3[5] and the IR and visible spectra of $(CF_3)_3CH$.[7] The $N = 5$ polyad has been measured at higher resolution using FT spectra in the present work and at high resolution *and* low pressure by Campargue and Stoeckel.[20] However, a complete coverage of the whole spectral range is necessary for a satisfactory analysis and understanding.

B. Assignment of the spectra by means of predictions from the effective Fermi resonance Hamiltonian

The visible spectra of CHF_3 were predicted by the tridiagonal Fermi resonance Hamiltonian[5] and assigned correspondingly. Briefly, we define a chromophore quantum number N for the stretching (v_s) *and* bending (v_b) vibrations:

$$N = v_s + \tfrac{1}{2}v_b. \tag{1}$$

The effective spectroscopic Hamiltonian (in cm^{-1} units) is block-diagonal in N and has the diagonal elements

$$H^N_{nn} = \tilde{\nu}'_s v_s + \tilde{\nu}'_b v_b + x'_{ss} v_s^2 + x'_{bb} v_b^2 + x'_{sb} v_s v_b + g'_{bb} l_b^2. \tag{2}$$

The nonzero off-diagonal elements are

$$H^N_{v_s v_b l_b;(v_s-1),(v_b+2),l_b} = -\tfrac{1}{2}k_{sbb}\left[\tfrac{1}{2}v_s(v_b - l_b + 2)(v_b + l_b + 2)\right]^{1/2}. \tag{3}$$

By diagonalizing this Hamiltonian one obtains the theoretical results for spectroscopic term values and relative band intensities within one polyad:

$$g_j = G_j / \sum_{\text{polyad}} G_k, \tag{4}$$

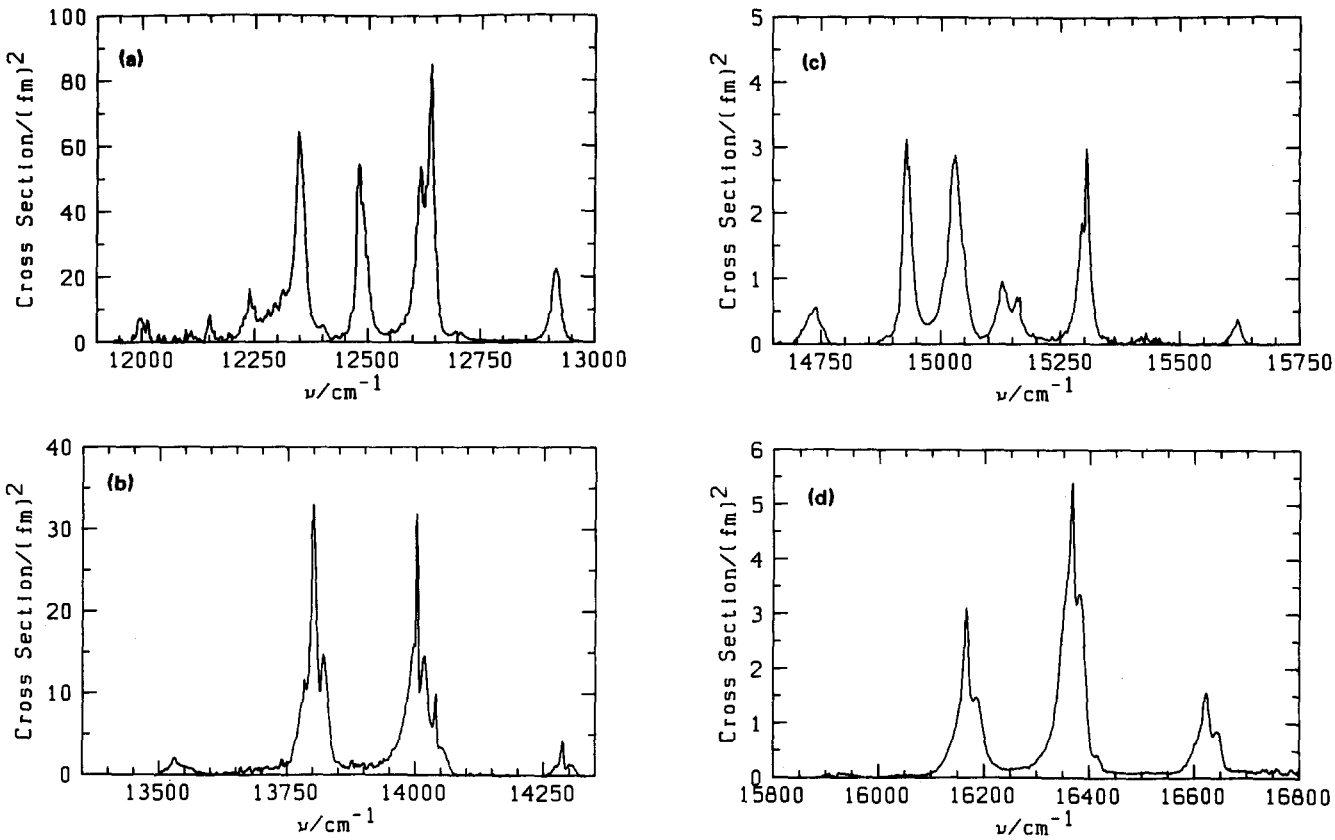

FIG. 1. Survey of the photoacoustic spectra of CHF_3 in the visible (experimental bandwidth $\simeq 2$ cm^{-1}). (a) Range corresponding to $N = 9/2$. (b) Range corresponding to $N = 5$. (c) Range corresponding to $N = 11/2$. (d) Range corresponding to $N = 6$. See also detailed discussion in the text concerning the evaluation of cross sections, etc.

$$G_k = \int_{\text{band } k} \sigma(\tilde{\nu}) \frac{d\tilde{\nu}}{\tilde{\nu}}. \tag{5}$$

With a theoretical dipole moment function for the CH chromophore, one also obtains the absolute intensities discussed in Sec. III D. The origin and interpretation of the effective tridiagonal Fermi resonance Hamiltonian has been discussed in substantial detail elsewhere.[5,26] Table I shows its success in predicting and fitting the visible spectra of CHF_3. The column pred. $\tilde{\nu}$ contains true predictions of frequencies for all polyads with $N \geqslant 9/2$, which were obtained on the basis of FTIR spectra and two bands from Ref. 1 [5_2 and $(9/2)_2$] in the absence of knowledge of the other bands.[5] The predictions are seen to be very satisfactory, with slightly increasing discrepancies for the highest polyads. A global fit to all 35 bands (FTIR and visible spectra) gives some improvement, quantitatively, but no change in the interpretation. We note that both frequencies and relative band intensities were well predicted and fitted.

In the assessment of the experimental results and comparison with theory one must realize that in the absence of a rotational fine structure analysis in the visible spectra the band centers can be determined only to within a few cm^{-1}, taking into account also some uncertainty in the frequency calibration procedure. Because rotational fine structure seems to be absent even at much higher resolution,[20] it might be impossible in the future to obtain much more accurate data for the band centers.

Table II summarizes the parameters of the effective Hamiltonian which were obtained by various evaluations of the data. The first two columns are from a global fit to all data. The first takes the band at 14 003 cm^{-1} as primary data in the fit, whereas the second fit B takes the local Fermi resonance occuring in this band into account (see Sec. III E 3 for a detailed discussion of this point). In view of what we have said above about the accuracy of band centers, a root mean square deviation of 4 cm^{-1} for 35 bands is excellent. It may be compared with a rms deviation of 1.9 cm^{-1} for the fit to the 22 IR bands only (third column, Ref. 5) and also to the rms deviation of 11 cm^{-1} found for our fit to 31 IR and visible bands of $(CF_3)_3CH$.[7] Taking also into account the excellent agreement of experiment and theory concerning the relative intensities, the CHF_3 spectra are clearly the largest and best understood data set of this kind, so far. It is seen that the model parameters vary only slightly for the various fits, including in this consideration also the fit of only 15 bands, using the same model, performed in Ref. 20 (last column in Table II). The fourth column in Table II is from converged variational calculations on the basis of CH stretch–CH bend normal mode force field to fourth order, which has been shown to be equivalent to the effective spectroscopic Hamiltonian in Ref. 26. The calculations of Ref. 26

TABLE I. Overtone spectra of the CH chromophore in CF_3H.

N	j	Expt. $\tilde{\nu}/cm^{-1}$	Footnotes		Pred. $\tilde{\nu}/cm^{-1}$	Fit $\tilde{\nu}/cm^{-1}$	g(expt)	g(fit)
(A) A_1 polyads (FTIR and photoacoustic spectra)								
4	1	11 563	a,b	(FT)	11 563	11 558	0.18	0.22
	2	11 347	a,b	(FT)	11 344	11 351	0.66	0.63
	3	11 109	a,b	(FT)	11 108	11 112	0.16	0.14
	4	10 777	j	(FT)	10 774	10 774	···	0.01
	5	···			10 359	10 350	···	0.000 1
5	1	14 289	c	(FT)	14 298	14 282	0.03	0.05
	2	14 003	c,d	(FT)	14 009	14 012	0.46	0.42
	3	13 800	c	(FT)	13 790	13 803	0.48	0.47
	4	13 532	c	(PA)	13 529	13 536	0.03	0.06
	5	···			13 179	13 177	···	0.002
	6	···			12 753	12 738	···	0.000 02
6	1	···			16 993	16 963	···	0.007
	2	16 621	e		16 639	16 629	0.17	0.11
	3	16 368	e		16 354	16 367	0.56	0.52
	4	16 164	e		16 132	16 154	0.27	0.33
	5	···			15 860	15 870	···	0.03
	6	···			15 501	15 498	···	0.000 7
	7	···			15 072	15 050	···	0.000 006
(B) E polyads (FTIR and photoacoustic spectra)								
9/2	1	12 917	f,g		12 922	12 911	0.08	0.21
	2	12 652	f,g		12 637	12 639	0.45	0.56
	3	12 351	f,g		12 349	12 352	0.42	0.21
	4	11 999	g		11 998	11 996	0.05	0.02
	5	···			11 574	11 563	···	0.000 3
11/2	1	15 619	i		15 643	15 621	0.03	0.06
	2	15 302	h,i		15 311	15 307	0.32	0.38
	3	15 025	i		15 023	15 031	0.52	0.45
	4	14 735	i		14 723	14 729	0.13	0.10
	5	···			14 361	14 358	···	0.006
	6	···			13 930	13 912	···	0.000 08

[a] FTIR data, band maxima determined from photoacoustic spectrum are: 11 565, 11 347, and 11 110 cm^{-1}. The band centers in all bands are shifted from the maxima at most by a few cm^{-1} (see discussion in Sec. III D).

[b] Reference 19 gives 11 562, 11 401, and 11 110 cm^{-1}. 11 401 cm^{-1} is possibly a misprint. A value close to 11 350 seems more probable from the figure given in the reference.

[c] FT and photoacoustic data as indicated. Reference 19 gives band maxima at 14 290, 14 003, 13 801, and 13 530 cm^{-1}. Reference 20 has band maxima at 14 290.7, 14 002.9, 13 800.7, and 13 532.4 cm^{-1}.

[d] For the fit a value of 14 012 cm^{-1} was adopted to correct for a local resonance with the state at 14 040 cm^{-1}. See the text (Sec. III D in particular).

[e] Reference 19 has band maxima at 16 614, 16 362, and 16 158 cm^{-1}.

[f] Reference 19 has band maxima at 12 925, 12 641, and 12 347 cm^{-1}.

[g] Additional bands appear at 12 485, 12 240, and 12 152 cm^{-1}. See the text and Table III for assignment.

[h] Reference 19 gives 15 298 cm^{-1}.

[i] Additional bands at 15 162/15 156, 15 125, and 14 928 cm^{-1}. See the text and Table III for assignment.

[j] Weak band with poor signal to noise (about 4:1), not included in the fit, as the assignment of the band center is very approximate.

included all couplings between stretching and bending vibrational states, but disregrading explicit resonance couplings to any other vibrational modes.

Table II shows that the parameters of the model Hamiltonian are stable with respect to slight changes of the description, of the fitting procedure or the data set used. This is evidence that the important physical phenomena are well represented by the effective Hamiltonian parameters. The only exception to this may be the parameter g'_{bb}, which would appear to be poorly determined. The variations found in Table II for all the other parameters give a good indication to what extent these are physically well determined. Of course, the uncertainties derived for the parameters from any single one of the least square fits are smaller, but they do not have much physical significance and are therefore not reproduced here. In particular, the large value of the effective spectroscopic constant $k_{sbb} \approx 100$ cm^{-1} ($\pm 10\%$ at most) is now very well established. It remains essentially identical to our first approximate determination from band intensity measurements[3] ($k_{sbb} = 99$ cm^{-1}, corresponding to a coupling matrix element $W = 70$ cm^{-1} in the $N = 1$ dyad), but now it is based upon very strong experimental evidence from an unprecedented data set. We still need to discuss a few bands, which were not included in our evaluation, because they have an assignment involving other vibrational modes.

TABLE II. CHF_3 parameters for the tridiagonal Fermi resonance Hamiltonian.

	Fit A[a]	Fit B[b]	Ref. 5[c]	Fit C[d] (Ref. 26)	Ref. 20[f]
$\tilde{\nu}_s'/cm^{-1}$	3078.58	3078.67	3079.8	3079.06	3079.3
$\tilde{\nu}_b'/cm^{-1}$	1379.58	1379.58	1377.8	1380.704	1381.0
x_{ss}'/cm^{-1}	− 60.00	− 59.93	− 61.7	− 60.19	− 60.8
x_{sb}'/cm^{-1}	− 26.87	− 27.27	− 28.6	− 25.47	− 28.7
x_{bb}'/cm^{-1}	− 7.48	− 7.42	− 6.5	− 7.85	− 4.2
g_{bb}'/cm^{-1}	5.40	5.21	4.5	0.84	...
k_{sbb}/cm^{-1}[e]	(±)100.01	(±)100.43	(±)106.1	(±)98.87	(±)105.8
rms/cm^{-1}	4.24	3.89	1.9	4.46	1.55[g]
No. of data[h]	35	35	22	35	15

[a] FTIR and photoacoustic spectra without corrections on band centers. $N \leqslant 6$.
[b] FTIR and photoacoustic spectra. Band at 14 003 cm^{-1} corrected for local Fermi resonance. $N \leqslant 6$.
[c] FTIR data. $N \leqslant 5$.
[d] Band centers and relative intensities from a variational calculation in normal coordinate basis and a polynomial or equivalent Morse expansion for the potential (see Ref. 26 for details).
[e] The sign of k_{sbb} is undetermined.
[f] Only parallel bands. $N \leqslant 5$.
[g] Calculated from the standard deviation given in Ref. 20.
[h] The rms is the root mean square deviation between experimental and theoretical values for these bands. Note that for the sets with 35 bands high overtone data are included using band maxima instead of band centers, which introduces by itself errors of a few cm^{-1} at most (see Sec. III E). One very weak band is not included in the fit. The relative intensities provide additional data, that are not counted in this number.

C. Assignment of bands involving the CF_3 stretching vibrations

Whereas at low frequencies corresponding to less than 6000 cm^{-1} several bands appear that clearly do not belong to the CH stretching and bending polyads, only few such bands occur in the high frequency spectra. Indeed, in the spectral regions of the dominant absorption corresponding to integral N no bands of comparable intensity remain unassigned, when we just consider the CH polyads. However, in the ranges of the half-integral N polyads the absorption is intrinsically weaker and some bands of about similar strength are not predicted by the simple effective Hamiltonian. A total of eight such bands observed above 7000 cm^{-1} are collected in Table III together with some low frequency bands that are relevant for the assignment. In the interpretation of these bands two main possibilities have been investigated among others: (i) the bands arise through strong coupling with other CH stretch bend states of different l_b (i.e., violating the $\Delta l_b \neq 0$ selection rule of the simple model). (ii) The bands arise as combination tones with the two CF_3 stretching vibrations ν_2 and ν_5 which form a strongly Coriolis coupled pair.[27,28]

In order to avoid a possibly fallacious assignment of these last few unassigned bands of the overtone spectrum we have considered this question in some detail and have finally rejected the first possibility and accepted the second on the following grounds: No adequate set of parameters could be found to fit the bands with a Hamiltonian allowing for $\Delta l_b \neq 0$ bands. Furthermore, the assigned bands are all very well predicted, which would imply that strong further interactions are unlikely. On the other hand, for the lower frequency bands up to 10 000 cm^{-1}, the rotational contours of the extra bands provide clear evidence in favor of the combination tone assignment, although we have not yet performed a detailed rotational analysis (see also Sec. III D of Ref 5). The frequency and intensity match of the predicted bands is also very satisfactory for this assumption, when we note that for the predictions in Table III the x_{ij} have been neglected and only the sums of the observed term values N_j with ν_2 and ν_5 have been calculated, without diagonalization of the new sum polyad Hamiltonian (there are not enough data available to justify this more correct procedure). We thus con-

TABLE III. Bands assigned to combinations with the CF_3 stretching vibration.

		Assignment to $N_j + \tilde{\nu}_{CF_3}$	
$\tilde{\nu}_{obs}/cm^{-1}$	$\tilde{\nu}_{pred}/cm^{-1}$	N	j
1 142	(ν_2)	0	0
1 158	(ν_5)	0	0
4 160	4 176/4 193	1	1
3 850	3 851/3 868	1	2
7 103	7 100/7 117	2	1
6 853	6 851/6 868	2	2
9 940	9 934/9 951	3	1
9 730	9 730/9 747	3	2
12 700	12 704/12 721	4	1
12 485	12 488/12 505	4	2
12 240	12 250/12 267	4	3
15 425	15 430/15 447	5	1
15 138[a]	15 144/15 161	5	2
14 930[b]	14 941/14 958	5	3

[a] Doublet 15 125/15 156 cm^{-1}.
[b] With structure, estimated center.

firm the previous assignment of combination tone transitions also for the higher polyads in the visible spectra. With this, no strong bands remain unassigned in the near IR and visible spectrum of CHF_3.

A question that remains is the origin of the *intensity* of the combination tones. One may first note that the E combination term can interact with the E terms of the half-integral N polyads. But also, and perhaps more likely, the very intense CF_3 stretching vibration may have intense combinations with the CH chromophore in its own right by a mechanism similar to the one proposed for the half-integral N polyads themselves.[26] The normal modes ν_5 and ν_4 mix of course internal coordinates of CH bending CF_3 stretching character. It is somewhat unfortunate that the high overtone bands have not enough definite rotational structure to provide final proof of our assignment for the combination tone assignment. However, the rotational contours do contain some additional relevant information, which we shall discuss after consideration of the band strengths.

D. Band strengths and effective dipole moment functions

Table IV summarizes band strength data, summed over complete polyads

$$G_N = \sum_k G_{N_k}.$$

These data are compared with theoretical results derived from the simple local Mecke model for the CH dipole moment function[16–18]:

$$\mu(r) = cr^m e^{-\alpha r},$$

where $\alpha = m/r_m$, and in our case $m = 1$.Two different choices r_m, the location of the maximum of the dipole function, were found to be adequate, $r_m/r_e \simeq 0.64$ and $r_m/r_e \simeq 6$ (or generally quite large).[17] It is seen that the second choice leads to good agreement in the band strengths of the higher overtones, whereas the first choice is somewhat better for the first overtone and still acceptable for the higher overtones. From the data, no definite conclusion can be reached. One should also consider here the obvious experimental uncertainties and discrepancies. Although the values from individual techniques are very well reproducible, the results for the $N = 5$ polyad with different techniques cover a substantial range of values for G.

We have generally found that for the FTIR measurements a total error of about 30% may be possible and it would appear that the actual systematic error in the photoacoustic measurements may be larger, particularly in view of the necessary calibration (see Sec. II). We thus must be satisfied at present with the accuracy available in Table IV, which is probably about as accurate (or more) as any data available in the literature for polyatomic molecules, where mostly a comparison of different techniques with their various systematic errors has not been possible. We conclude that at present the nature of the effective dipole moment function remains undetermined. Work is in progress to provide a better theoretical understanding.[50] The present data, together with those for $(CF_3)_3CH$[7] provides a first step towards a systematic, relatively complete data base for the isolated CH chromophore.

TABLE IV. Total band strengths for the CH overtone polyads.

	$G/(\text{fm})^2$			
			Theory	
N	Experiment	Ref.	Mecke A[a]	Mecke B[b]
1	133 000	(2,5,c)	133 000	133 000
2	240	(5,c)	359	1 865
3	44	(5,c)	3.9	60
4	3.6	(5,c,g)	3.0	3.2
4.5	0.55	d		
5	0.36	e	0.67	0.24
	0.27	(20)		
	0.19	d		
5.5	0.015	d		
6	0.027	d,f	0.13	0.023

[a] Using $r_m/r_e = 0.64$ (see Refs. 16–18).
[b] Using $r_m/r_e = 6$ (see Refs. 16–18).
[c] FTIR data (Refs. 2 and 5).
[d] This work, photoacoustic data.
[e] This work, FTIR data.
[f] Reference 19 quotes 0.073 fm^2, but apparently for the band at 16 629 cm^{-1} which contains only about 17% of the intensity. If this is taken into account, one would obtain $G = 0.43$ fm^2. The origin of the discrepancies is not clear.
[g] The value from the photoacoustic measurements is 2.5 fm^2.

E. Rotational constants and band contours

Although no rotational line structure appears in the visible spectra under the conditions of our experiments, the band contours contain additional information concerning both the symmetry assignment of the bands and the rotational constants, which are strongly influenced by the Fermi resonance. Our analysis proceeds according to the following three steps:

(i) From an analysis of the $2\nu_{4(b)}$ (E) component we derive the "unperturbed" bending rotational constants, in particular a value for α_b^B.

(ii) From an analysis of the rotational fine structure in the low frequency bands (up to $N = 7/2$) we derived a value for α_s^B.

(iii) Finally, we predict and simulate the high frequency Fermi resonance bands ($N \geqslant 4$) introducing additional effects as necessary in order to understand the bands.

1. Analysis of $2\nu_b(E)$

Figure 2 shows the rotational fine structure of the perpendicular component of the overtone of the CH bending vibration. It has been assigned and fitted using the following term formula for the rovibrational states[29,30] (when $l = \pm 1$):

$$\begin{aligned} F(J,K) = {} & \tilde{\nu}_0 + BJ(J+1) + (C-B)K^2 \\ & \mp 2C\zeta_{\text{eff}}K \\ & - D_J J^2(J+1)^2 - D_{JK}J(J+1)K^2 - D_K K^4 \\ & \pm \eta_{\text{eff}}^J J(J+1)K \pm \eta_{\text{eff}}^K K^3. \end{aligned} \quad (6)$$

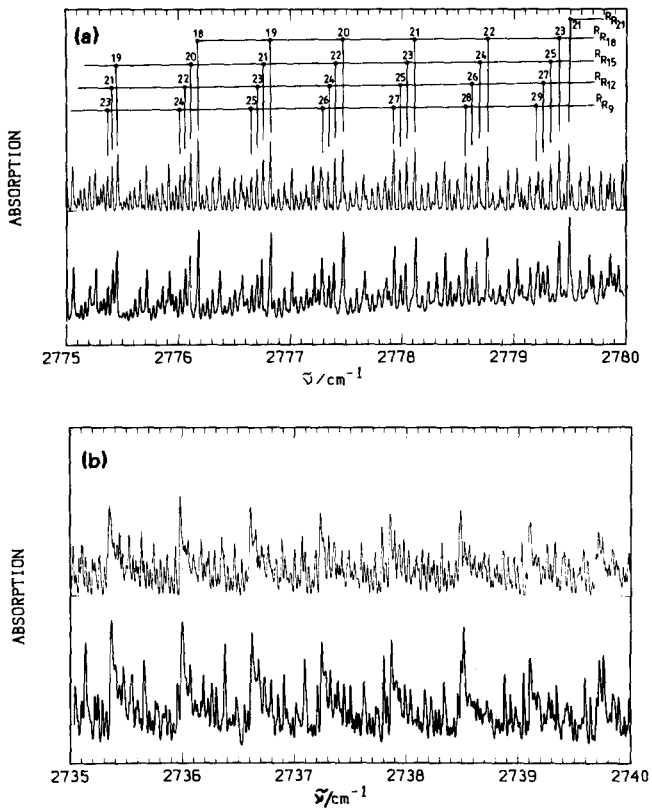

FIG. 2. High resolution spectrum in the range of the first overtone of the CH bending vibration (effective spectral bandwidth 0.014 cm^{-1}) using a 20 m long path absorption cell. The lower trace is the simulated, the upper the experimental spectrum. (a) Range of the ^RR branch with some sample assignments. (b) Range of the overlapping spectra of $2\nu_4(E)$ and $(1)_2(A_1)$.

The upper (lower) sign is valid for the $+l(-l)$ level (cf. Ref. 29, Fig. 103).

A total of 317 assigned lines (mostly from the R_R branch with $K'' \leqslant 24$, $J'' \leqslant 32$) were introduced into a least squares fit,[39] the ground state constants being fixed. The results are summarized in Table V. From the analysis of the CH bending fundamental a value of $\zeta_{\text{eff}} = -2\zeta_b = -1.9689$ is expected from the harmonic sum rule.[31,53]

TABLE V. Least squares parameters from the simulation and fit[a] of $2\nu_b(E)$ (giving statistically significant digits).

	$2\nu_b(E)$	Ground state[b]
$\tilde{\nu}_0$/cm^{-1}	2754.796[c]	0
B/cm^{-1}	0.344 387	0.345 201 05
C/cm^{-1}	0.189 09	0.189 25
ζ_{eff}	−1.964 5	...
$D_J/10^{-7}$ cm^{-1}	3.93	3.779
$D_{JK}/10^{-7}$ cm^{-1}	−3.7	−6.037 5
$D_K/10^{-7}$ cm^{-1}	3.9[d]	3.72
$\eta^J_{\text{eff}}/10^{-6}$ cm^{-1}	−1.9	...
$\eta^K_{\text{eff}}/10^{-6}$ cm^{-1}	5.5[d]	...

[a] The root mean square deviation for 317 lines was 3×10^{-3} cm^{-1}.
[b] The ground state constants from Refs. 31, 34, and 35 were kept fixed in the fit.
[c] For the absolute wave number calibration we used HCl lines from Ref. 36.
[d] D_K and η^K are correlated in the fit (see also Ref. 54).

This is in good agreement with our result as well as α^B_b (4.127×10^{-4} cm^{-1} in Ref. 31 compared to $\alpha^B_b = 4.070\times10^{-4}$ cm^{-1} from Table V). The value of α^B_b can thus be considered to be well established both from the fundamental and first overtone spectrum of the CH bending vibration. Previously, only low resolution results were available for the E component of the overtone.[32,33] Because of the resonances occuring in ν_1 and the interaction with $2\nu_b(A_1)$[3] one cannot use the rotational constants of the Fermi resonance components $(1)_1$ and $(1)_2$[5] in order to determine α^B_b, before the complete band system is understood in detail.

Before proceeding to determine α^B_s, we mention a further result from our analysis of $2\nu_b(E)$. In the region between 2730 and 2740 cm^{-1}, which is shown in part in Fig. 2(b), there is overlap between the parallel (2710 cm^{-1}) and perpendicular (2755 cm^{-1}) components of $2\nu_b$. By simulating the overlap between the two components in Fig. 2(b) we could determine the ratio of band strengths, approximately:

$$\frac{G(2710\text{ cm}^{-1})}{G(2755\text{ cm}^{-1})} \simeq 6 \pm 0.5$$

and therefore[5]

$$G(2755\text{ cm}^{-1}) \simeq (1 \pm 0.3)\times10^{-3}\text{ pm}^2.$$

The large ratio justifies our earlier use of the band strengths of 1_2 and 1_1 to determine the Fermi resonance coupling matrix element.[3]

2. Determination of α^B_s from an analysis of the Fermi resonance component bands

In general, the analysis of the rotational fine structure of Fermi resonance components proceeds by adding the rotational term values to the diagonal matrix elements in Eq. (2) using the expansions (for B and C similarly)

$$B_{v_1v_2\cdots v_n} = B_e - \sum_{i=1}^{n}(v_i + \tfrac{1}{2})\alpha_i. \tag{7}$$

Then one diagonalizes the Hamiltonian for each J and K, possibly introducing J and K dependent terms in the off-diagonal elements [Eq. (3)]. Such a procedure has been used, for instance, in Ref. 37 for CF_3I and Ref. 38 for CHD_3. In the present case a more approximate procedure is adequate, which we have checked numerically to be sufficiently valid for a very similar situation.[38]

Neglecting rotation, one has for the Nth block of the vibrational Fermi resonance Hamiltonian (eigenvector matrix Z):

$$\text{Diag}(E^N_{nm}) = \mathbf{Z}^T\mathbf{H}^N\mathbf{Z}. \tag{8}$$

Adding only the diagonal rotational term values $F(J,K,v_1\cdots v_n)$ to $\mathbf{H}^N$ one obtains (diagonal matrix of term $\mathbf{F}_D$)

$$\mathbf{Z}^T(\mathbf{H}^N + \mathbf{F}_D)\mathbf{Z} = \text{Diag}(E^N_{nm}) + \mathbf{Z}^T\mathbf{F}_D\mathbf{Z}. \tag{9}$$

The diagonal correction to the total energy is thus obtained from Eq. (10):

$$E_{mm} = E^N_{mm} + \sum_l |Z^N_{lm}|^2 F_{ll}. \tag{10}$$

The off-diagonal contribution to the energy in Eq. (9) is relatively small and neglected, if the vibrational Fermi com-

ponents are well separated compared to the rotational terms. The rotational term formulas are linear in the constants $X = B, C, D$, etc., hence one can express the energy in Eq. (10) as a vibrational contribution from each Fermi component m and a rotational contribution with the new, effective rotational constants X^F_m in the usual term formula:

$$X^F_m = \sum_l |Z^N_{lm}|^2 X_l, \tag{11}$$

X_l is computed according to Eq. (7). Applying these equations to the CH stretching and bending Fermi resonance component N_j with all other vibrations in the ground state one can write

$$\begin{aligned} B^F_{Nj} &= \sum_i |Z^N_{ij}|^2 B_i \\ &= B_0 - \alpha^B_s \sum_i |Z^N_{ij}|^2 v_{si} - \alpha^B_b \sum_i |Z^N_{ij}|^2 v_{bi}. \end{aligned} \tag{12}$$

The terms under the sums result from diagonalizing the vibrational Hamiltonian with v_{si} and v_{bi} being the stretching and bending quantum numbers for the basis state $|i\rangle = |v_{si}, v_{bi}\rangle$. Equation (12) may also be written in terms of "effective stretching and bending quantum numbers" appropriate for the Fermi resonance component j,

$$B^F_{Nj} = B_0 - \alpha^B_s v^{\text{eff}}_{sj} - \alpha^B_b v^{\text{eff}}_{bj}. \tag{13}$$

In these equations v^{eff}_{sj}, v^{eff}_{bj}, and α^B_b are thus known. We have obtained α^B_s from a least squares fit to rotational constants obtained from various Fermi resonance components, for which the rotational fine structure could be analyzed. These bands, their observed and calculated B values are summarized in Table VI. The corresponding value for α^B_s is $1.4\times10^{-4}\,\text{cm}^{-1}$. We have finally estimated also α^c_s, which is expected to be small, from the ratio α^B_b/α^B_s to be about $4\times10^{-5}\,\text{cm}^{-1}$. We have thus a set of rotational constants to predict at least roughly the rotational contours of the overtone spectrum. Together with known values for the α_i of other vibrations, our value for α^B_b and α^B_s permits us to estimate $B_e \simeq 0.347\,33\ \text{cm}^{-1}$ and $C_e = 0.190\,603\ \text{cm}^{-1}$. This completes to some extent the structural investigation of Bernstein and Herzberg[1] (see Table VII for the summary of current rovibrational constants). A definite analysis of deperturbed α values for CDF_3, which is not yet available but perhaps possible in the near future,[22] would provide the necessary information to derive an r_e structure. The best current r_0 structure for CHF_3 is $r_0(\text{CH}) = 109.58$ pm, $r_0(\text{CF}) = 133.312$ pm, $\alpha(\text{FCF}) = 108.6113°$, $\alpha(\text{HCF}) = 110.318°$ from these results, the digits given being not necessarily all physically relevant.

3. Prediction and analysis of the band contours of the high frequency bands

Starting with the $N = 4$ polyad, no rotational fine structure was observed, even under resolution and pressure broadening conditions, under which at least J structure should appear if the bands were simple. Figure 3 shows as a first example the simulation of the 4_2 component by means of predicted rotational constants. Although some details of the experimental spectrum remain undescribed, an adequate fit of the major contour, including in particular the Q-branch width and relative height compared to P and R branches, is obtained if one assumes an empirical Lorentzian linewidth $\Gamma = 2.7\,\text{cm}^{-1}$. This is to be compared with the approximate pressure broadening width of $0.4\,\text{cm}^{-1}$, which gives a simulated spectrum with a narrow Q branch and some rotational J structure.

Figure 4 shows as a second example the simulation of the 5_2 component, which shows some particularities. First, the band is clearly split by an additional, local Fermi resonance, which leads to the appearance of two Q-branch maxima at 14 003 and at 14 037 cm^{-1}. The interpretation of these Q branches as arising from a local Fermi resonance is supported by the band strengths (see below and Table I), and by the fact that the position of the 5_2 state in this local resonance is at 14 012.4 cm^{-1}, close to the predicted values in Table I (14 009 or 14 012 cm^{-1}, respectively). This Fermi resonance is taken into account in the simulation with the unassigned partner at 14 034.6 cm^{-1} and a local coupling matrix element of 15 cm^{-1}. Because of this additional resonance, the rotational constants have been adjusted in the fit and

TABLE VI. Rotational constants B of the Fermi resonance components.

State	$\tilde{\nu}_0/\text{cm}^{-1}$ [a]	$B_{\text{obs}}/\text{cm}^{-1}$	Ref.	$B_{\text{calc}}/\text{cm}^{-1}$	$v_{s,\text{eff}}$	$v_{b,\text{eff}}$	Remarks
$(1/2)_1$	1 377.9	0.344 788 35	31	0.344 79	0	1	b,c
$(1)_2$	2 710.2	0.344 5151	5	0.344 42	0.05	1.9	b,d
$2\nu_b(E)$	2 754.8	0.344 387	this work	0.344 38	0	2	b,c
$(2)_1$	5 959.4	0.344 75	5	0.344 75	1.82	0.35	b
$(2)_2$	5 710.4	0.344 65	5	0.344 23	1.02	1.97	b,d
$(3)_1$	8 792.5	0.344 33	1	0.344 38	2.49	1.03	e
$(3)_2$	8 589.3	0.344 23	1	0.344 09	2.04	1.92	e
$(7/2)_1$	10 155.9	0.343 6	5	0.343 84	2.36	2.27	f
$(7/2)_2$	9 881.9	0.341 0	5	0.343 40	2.02	2.96	f,d

[a] Rounded values.
[b] From high resolution spectra.
[c] Used to determine α^B_b (see the text).
[d] Not included in the fit because of additional resonances (see Refs. 3 and 5).
[e] From moderate resolution spectra, recalculated from the α^B_{eff} of Ref. 1 and the precise value $B_0 = 0.345\,201\,05$ of Ref. 35.
[f] From a band contour simulation of a pressure broadened spectrum.

TABLE VII. Summary of fundamental frequencies and rotation vibration constants α_i for CHF_3.

Nominal assignment	$\tilde{\nu}/cm^{-1}$	α_i^B / 10^{-4} cm^{-1}	α_i^C / 10^{-4} cm^{-1}	References
$\nu_1(A_1)$("s")	3020	1.4 ± 0.4	0.4	this work, a, 3, 5, d
$\nu_2(A_1)$	1141.457 77	4.116	4.7811	27, 40
$\nu_3(A_1)$	700.100 9	6.463	1.700	41
$\nu_4(E)$("b")	1372	4.1	0.8	this work, b
	1377.845 76	4.127	1.12	31, c
$\nu_5(E)$	1158.342 5	12.457	5.538	27, 40
$\nu_6(E)$	507.822 8	-1.217	3.418	41

[a] α is not derivable from the fundamental band (see the text), the fundamental frequency is from the effective Hamiltonian. The 1_1 component is at about 3035.5 cm^{-1}.
[b] From overtone $2\nu_4(E)$, the frequency is from the effective Hamiltonian.
[c] From fundamental.
[d] One can also calculate α_1^C from the average rotational constant when exciting the anharmonic fundamental in normal coordinate space, obtaining $\alpha_1^C = 6.7\times10^{-6}$ cm^{-1} and $\alpha_1^B = 4.7\times10^{-4}$ cm^{-1}, the latter being not in good agreement with experiment.

furthermore the hot bands with ν_6 added [one low frequency side peak is visible in the spectrum, most easily in Fig. 4(c)]. Our interpretation of the Fermi resonance is similar to Ref. 20 and the slight differences in the numerical parameters, which have been obtained independently, do not warrant discussion. Our simulation includes rotational structure and thus some shift $\tilde{\nu}_0 - \tilde{\nu}_{max}$. A feature that cannot be easily fitted is the P-branch height and decline to low frequencies. A similar feature will reappear below for the 6_4 component. The Lorentzian width in the fit is 1.25 cm^{-1}, smaller than for 4_2. However, as also visible in Fig. 1(b), the Q branch of the 5_3 component is broad, about 11 cm^{-1} with an only slightly smaller Lorentzian width. These phenomenological widths are thus quite different for different members of the same polyad. Also, the shapes are often markedly non-Lorentzian, for instance the 5_3 Q branch is "flat" in the FT spectra.

Figure 5 shows experimental and simulated results for the 6_4 band. This band shows an effect, which appears already in the members of the $N = 5$ polyad but becomes now more pronounced. The P branch is strongly degraded to the low frequency side and shows no clear separation from the relatively broad Q branch, whereas the R branch still appears strongly with a separate maximum. This can be simulated rather well by adjusting the rotational constants [Fig. 5(b)]. The effect is present, but much weaker with the predicted rotational constants [Fig. 5(c)]. It can be due either to the limited validity of the Fermi resonance model in the higher polyads or due to interaction with further states with different rotational constants (the "background" states, which may be responsible for the phenomenological width $\Gamma = 6.5$ cm^{-1} in this case). This point will be discussed in the more general context below.

We conclude this section with an example from the perpendicular bands. Figure 6 shows the $(11/2)_4$ component. The simulation parameters are discussed in the caption and include a variation of ζ_{eff}, which is possible, although it was not necessary to invoke this effect in the simulations of the resolved perpendicular bands in the IR.[5] The structure of the perpendicular bands is somewhat indefinite, in general. It may be noted, though, that the structure of the combination tones as assigned in Table III seems to be systematically different from the perpendicular polyad components. Nothing definite can be concluded, at present, concerning the existence or absence of interaction between these band systems. It may be that data at higher resolution would help in the assignment, although this seems unlikely because of the generally large phenomenological widths needed to fit the spectra (i.e., $\Gamma > \Delta$ even with large Δ). It is now appropriate to discuss the origin and significance of the phenomenological widths that are found invariably in all of the high overtones.

F. Separation of time scales and mode selective vibrational redistribution

For all the high frequency polyads with $N \geq 4$ it was necessary to assume in the fit some phenomenological width. These widths are variable within the polyads and show a tendency to increase with the polyad number N. For instance, with $N = 4$ they are between about 1.5 and 3 cm^{-1}, for $N = 5$ between about 1 and 10 cm^{-1}, and for $N = 6$ about 7 cm^{-1}. As inhomogeneous rotational (and in several cases also vibrational hot band) structure has been taken into account in the determination of these widths, they are clearly due to homogeneous rovibrational structure (in the sense of Ref. 4). We rule out exceptional pressure broadening. The detailed nature of this structure cannot be obtained from our spectra. There is no evidence that it corresponds to a smooth Lorentzian, although this function has been used in the fitting. In some bands one can recognize some specific, non-Lorentzian, structure. The local Fermi resonance with $W \simeq 15$ cm^{-1} in the 5_2 component is an extreme example. Usually, the structure appears on the order of the widths quoted. The variations within one polyad and among the polyads are similar to $(CF_3)_3CH$,[7] where, however, the widths were by more than an order of magnitude larger and in part inhomogeneous. Also, the band profiles were perfectly smooth. The rougher structure for CHF_3 can be under-

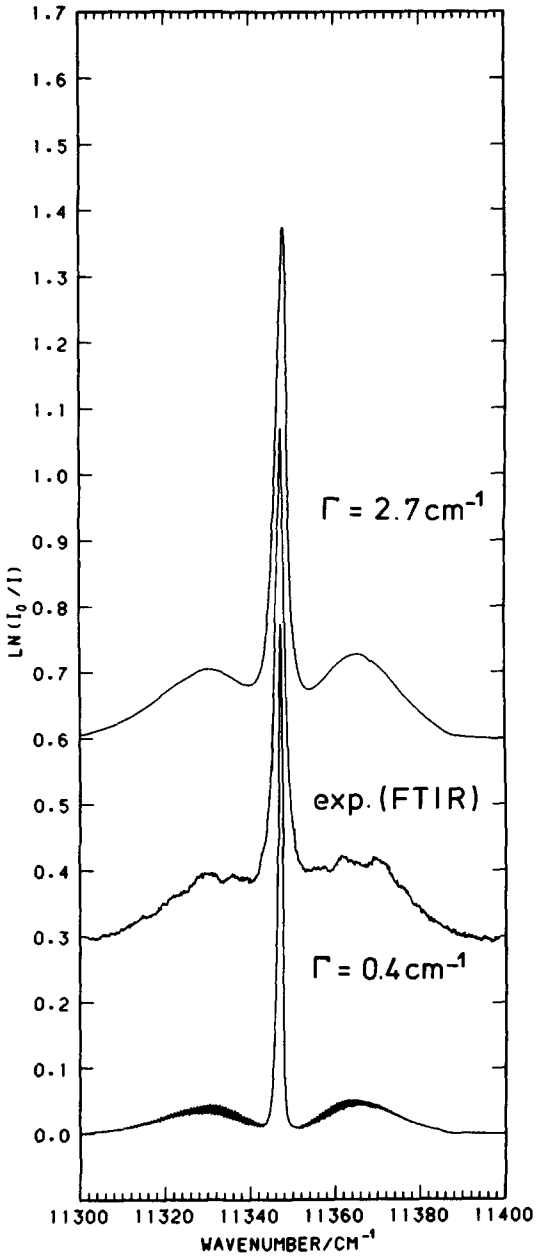

FIG. 3. Experimental trace and simulation of the 4_2 Fermi resonance component compared to experiment with Lorentzian widths Γ (FWHM) as indicated. The resolution is 0.2 cm^{-1} and the rotational constants have been predicted from the Fermi resonance model to be $B' = 0.343\,983$ cm^{-1}, $C' = 0.188\,897$ cm^{-1}. In the simulations the band center is shifted from the maximum by $\tilde{\nu}_0 - \tilde{\nu}_{max} = 0.5$ cm^{-1} ($\Gamma = 2.7$ cm^{-1}) and 0.7 cm^{-1} ($\Gamma = 0.4$ cm^{-1}), respectively. The base lines are shifted by 0.3 units in the upper spectra. Additional measurements at 210 K indicate that the weak band at 11 357 cm^{-1} is not a hot band, as it emerges more clearly at low temperature, whereas the high frequency bumps around 11 365 to 11 370 cm^{-1} become weaker at low T. No J structure is seen at low T and about 10^5 Pa pressure (0.2 cm^{-1} bandwidth).

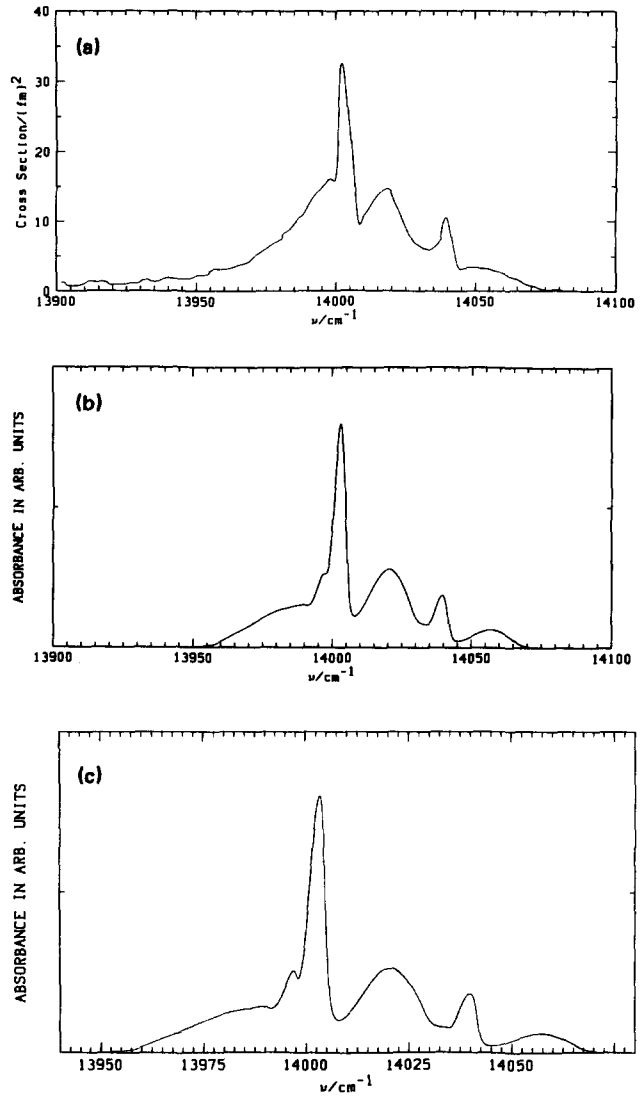

FIG. 4. Experimental and simulated spectra of the 5_2 component. (a) Experiment (resolution $\Delta \simeq 2$ cm^{-1} FWHM). (b) Simulation using two Fermi coupled states centered at 14 012.4 and 14 034.6 cm^{-1} (coupling matrix element $W = 14.8$ cm^{-1}) with rotational constants $B' = 0.341(0.340)$ and $C' = 0.188(0.187)$ cm^{-1}, width $\Gamma = 1.25$ cm^{-1}, resolution $\Delta = 2.0$ cm^{-1} (FWHM). Furthermore, hot bands were added at $\tilde{\nu}_{hot} - \tilde{\nu}_0 = -7.95(0.17)$, $-10(0.07)$, and $-16(0.02)$ cm^{-1} (relative intensity in parentheses). The band centers in the simulation are at 14 005 and 14 042 cm^{-1} compared to the band maxima at 14 003 and 14 039.5 cm^{-1}. (c) Simulation at high resolution ($\Delta \ll \Gamma$) showing clearly the appearance of the hot band (cf. also Ref. 20). All the other parameters are identical to (b), also including the shifts $\nu_0 - \nu_{max}$.

stood in terms of the densities of states shown in Fig. 7. Around 14 000 cm^{-1} the density of vibrational states of A_1 symmetry is about 50 per cm^{-1}, which could be coupled by anharmonic resonance. For the 5_2 component about this number of vibrational states might contribute to the phenomenological width at $J = 0$. For low J the density increases about with $2J + 1$, if one takes rovibrational couplings into account in the density $\rho(E, J, \Gamma_K)$ as first suggested in Ref. 42. These numbers are not too large to prevent resolution of individual lines with improved techniques, which are not accessible to us at the present moment. The prospects are, however, rather favorable, because certainly not *all* states will contribute equally. Even if only few states interact by very close resonances, as shown for the CH stretching fundamental of CHF_3,[3] the detailed analysis may prove very difficult without jet cooling.[47–49]

However, even without detailed rovibrational analysis a positive minimal statement is possible: *The homogeneous vibrational structure is not wider than about 1 to 10 cm^{-1},*

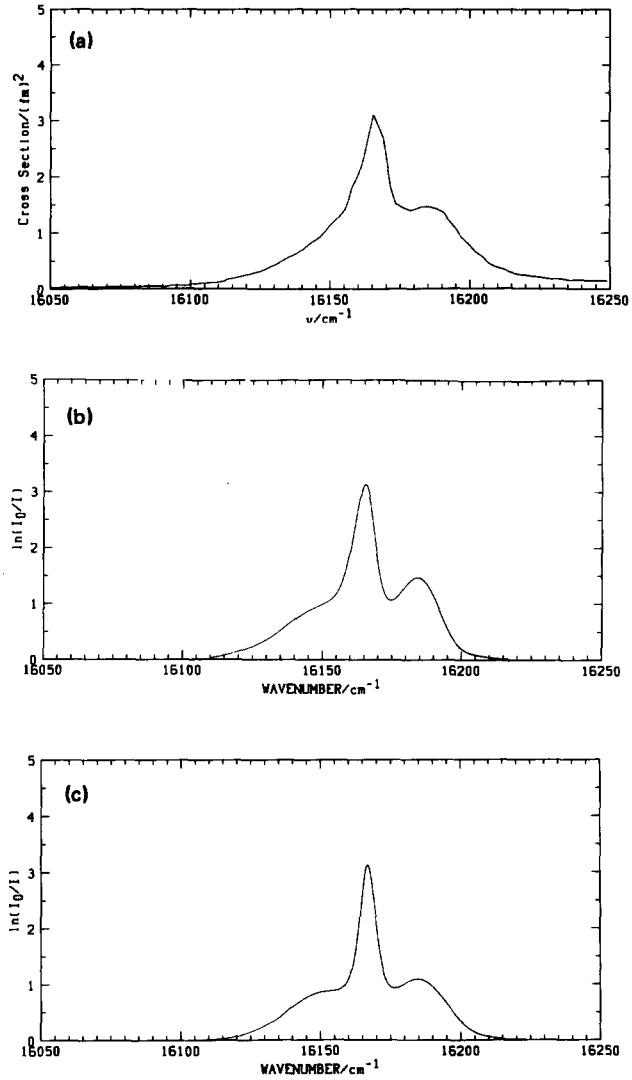

FIG. 5. Experimental and simulated spectra of the 6_4 component. (a) Experiment (resolution $\Delta = 2\ \text{cm}^{-1}$ FWHM). (b) Simulation with adjusted rotational constants $B' = 0.341\ \text{cm}^{-1}$ and $C' = 0.187\ \text{cm}^{-1}$, Lorentzian width $\Gamma = 6.5\ \text{cm}^{-1}$ (FWHM) and resolution $\Delta = 2\ \text{cm}^{-1}$. The shift between band center and band maximum is $\tilde{\nu}_0 - \tilde{\nu}_{\max} = 2.5\ \text{cm}^{-1}$. (c) Simulation with predicted rotational constants $B' = 0.343\,092\ \text{cm}^{-1}$ and $C' = 0.188\,64\ \text{cm}^{-1}$ and $\Gamma = 6.5\ \text{cm}^{-1}$, $\Delta = 2\ \text{cm}^{-1}$, $\tilde{\nu}_0 - \tilde{\nu}_{\max} = 1.5\ \text{cm}^{-1}$.

depending upon the band and excluding the local resonance in 5_2. This corresponds to initial transfer and decay times of *longer than 0.5 to 5 ps.* On the other hand, transfer from the stretching to the bending motion occurs on a time scale of about 50 fs, that is 10 to 100 times faster than the slower motion mentioned above.[5,15] *The initial time evolution is thus highly mode selective with a pronounced separation of time scales.* It is interesting, although somewhat accidental, that for CHF_3 a similar separation of time scales for redistribution was already observed in the fundamental (50 fs and about 10 ps, with similar difficulties in assigning the long time component in Ref. 3). Such a separation of time scales with mode selective transfer was also observed in the overtone spectra of $CH(CF_3)_3$, where the quantitative separa-

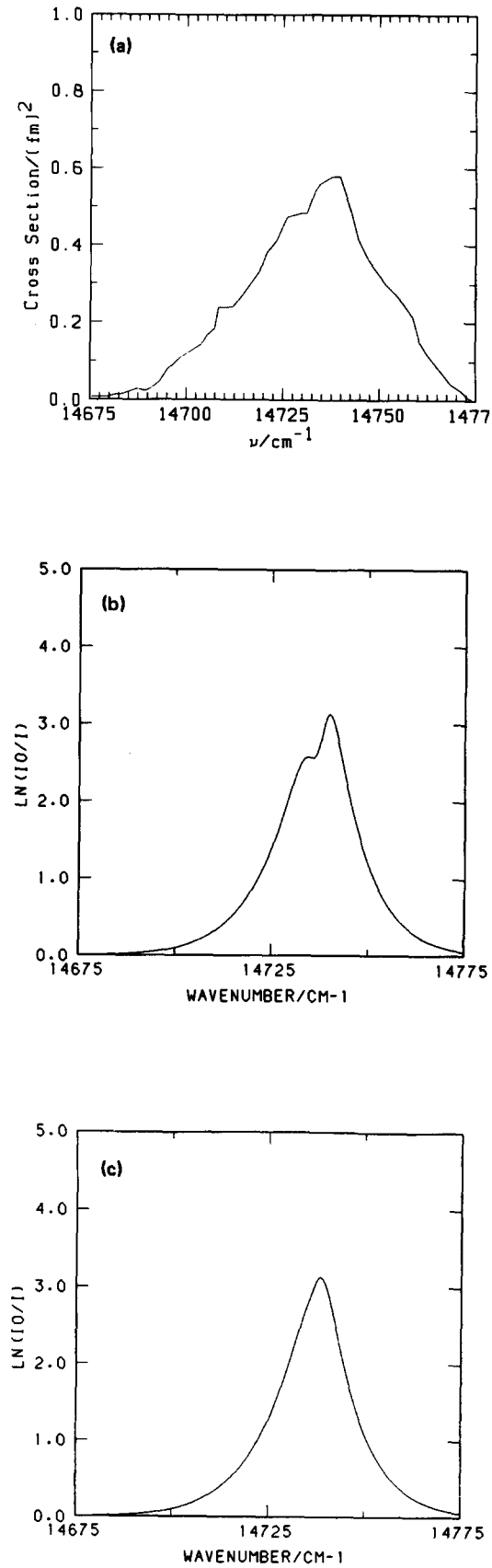

FIG. 6. Experimental and simulated spectra of the $(11/2)_4$ perpendicular component. (a) Experiment (resolution $\Delta = 2\ \text{cm}^{-1}$). (b) Simulation with predicted rotational constants $B' = 0.342\,483\ \text{cm}^{-1}$, $C' = 0.188\,461\ \text{cm}^{-1}$, $\Gamma = 4.0\ \text{cm}^{-1}$, and $\tilde{\nu}_0 - \tilde{\nu}_{\max} = -2\ \text{cm}^{-1}$. The value of ζ_{eff} has been taken to be 0.9 in this simulation. (c) Simulation as in (b) but with $\zeta_{\text{eff}} = 0.985$.

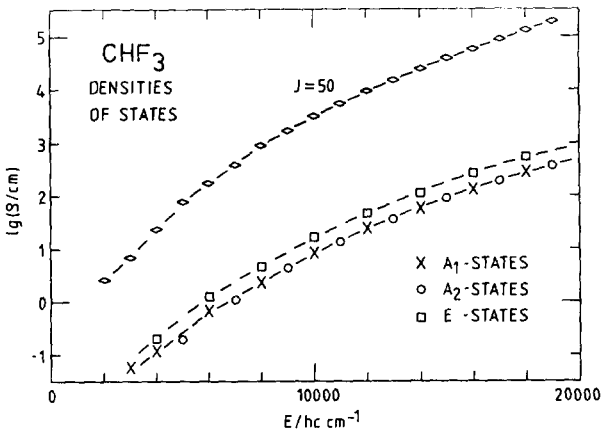

FIG. 7. Average densities of anharmonic rovibrational states ρ (averaged over 200 cm^{-1}) for CHF_3. The lower functions give the density of vibrational states of a given symmetry species in C_{3v}, which are approximately regular as calculated directly using algorithms developed earlier by us (see Refs. 43, 44, and also 45 and 46). The low energy part of the A_1 density had been reproduced in Ref. 3. The upper function gives $\rho(E, J=50)$. The corresponding $\rho(E, J, \Gamma_i)$ result from the regular property of the density. The fluctuations of $\rho(E, J, \Gamma_i)$ around the regular values for $J=50$ are smaller than for $J=0$ and thus not shown separately. (See Ref. 44 for a detailed discussion.)

tion is less pronounced.[7] The assignment of the long time dynamics remains open. One possibility might be an almost exponential decay into many states.[14] Another, perhaps more likely possibility involves a few state rovibrational interaction, which destroys any easily visible fine structure.

IV. CONCLUSIONS

Together with the data from Ref. 5, the present data allow us to obtain what is presumably the most complete assignment and detailed analysis of short time vibrational redistribution observable via the high overtone CH absorption spectra in polyatomic molecules. We can summarize our main conclusions:

(i) The tridiagonal Fermi resonance Hamiltonian provides quantitatively and qualitatively correct predictions for both the band positions *and* relative band intensities within the multiplets of bands that are observed in the visible overtone spectra of CHF_3 instead of one band that might naively be expected for each overtone state of the isolated CH chromophore. This finding provides further firm evidence that this type of interaction must be taken into account quite generally in the interpretation of the high overtone spectra of the alkyl CH chromophore.

(ii) The overtone intensities can be understood semiquantitatively on the basis of the phenomenological local Mecke dipole function.[16] The previously observed ambiguity[17,18] in the assignment of parameters for this function remains unresolved even with the advent of the present high overtone band strengths.

(iii) On the short time scale of <0.5 ps characteristic for the CH stretch bend Fermi resonance the approximate symmetric top Δl selection rule remains valid up to very high quantum numbers $N \leqslant 6$ for both the integral and half-integral N poyads in CH F_3. This is to be contrasted with the strong additional couplings that are observed in asymmetric top molecules.[8,9,51,52]

(iv) The overall rotational band contours can be qualitatively predicted on the basis of newly determined values for B_e, C_e, and rovibrational constants including the Fermi resonance interaction. In the higher overtones the differences between prediction and experiment become more marked, indicating mixing with states of very different rotational structure.

(v) In the near infrared and visible overtone spectra ($\tilde{\nu} > 11\,000$ cm^{-1}) no rotational fine structure is observed even under resolution and pressure conditions under which at least J structure should be observable in the parallel bands. This is further evidence for rovibrational homogeneous structure[4] in these bands. *Some* structure of this kind occurs even in the CH stretching fundamental.[2,3]

(vi) The additional homogeneous structure, as simulated phenomenologically by Lorentzian coarse shapes, occurs within frequency ranges of 1 to 10 cm^{-1}. It is different for the different polyads *and* for different bands within each polyad. In one case (5_2) a particular resonance could be identified but not assigned. Although the nature of the additional structure cannot be unraveled at present, it corresponds to redistribution times that are certainly longer than 0.5 to 5 ps, depending upon the band considered. This is to be compared with the proven CH stretch bend Fermi resonance redistribution, which occurs on a time scale, that is about one to two orders of magnitude faster. The expected separation of the time scales for mode selective vibrational redistribution and further evolution is thus present in CHF_3 and more pronounced than in $CH(CF_3)_3$.[7]

ACKNOWLEDGMENTS

Financial support of our work by the US and Swiss national science foundations is gratefully acknowledged.

[1] H. J. Bernstein and G. Herzberg, J. Chem. Phys. **16**, 30 (1948).
[2] H. R. Dübal and M. Quack, Chem. Phys. Lett. **72**, 342 (1980).
[3] H. R. Dübal and M. Quack, Chem. Phys. Lett. **80**, 439 (1981).
[4] K. von Puttkamer, H. R. Dübal, and M. Quack, Faraday Discuss. Chem. Soc. **75**, 197, 263 (1983).
[5] H. R. Dübal and M. Quack, J. Chem. Phys. **81**, 3779 (1984).
[6] S. D. Peyerimhoff, M. Lewerenz, and M. Quack, Chem. Phys. Lett. **109**, 563 (1984).
[7] J. E. Baggott, M.-C. Chuang, R. N. Zare, H. R. Dübal, and M. Quack, J. Chem. Phys. **82**, 1186 (1985).
[8] H. R. Dübal and M. Quack, Mol. Phys. **53**, 257 (1984).
[9] A. Amrein, H. R. Dübal, and M. Quack, Mol. Phys. **56**, 727 (1985); (to be published).
[10] E. L. Sibert, W. P. Reinhardt, and J. T. Hynes, Chem. Phys. Lett. **92**, 455 (1982); J. Chem. Phys. **81**, 1115 (1984).
[11] R. G. Bray and M. Berry, J. Chem. Phys. **71**, 4909 (1979).
[12] A. Amrein, H. Hollenstein, M. Quack, R. Zenobi, J. Segall, and R. N. Zare (to be published).
[13] H. R. Dübal and M. Quack, Chem. Phys. Lett. **90**, 370 (1982).
[14] M. Quack, Faraday Discuss. Chem. Soc. **71**, 359 (1981).
[15] R. Marquardt, M. Quack, J. Stohner, and E. Sutcliffe, J. Chem. Soc. Faraday Trans. 2 **82**, 1173 (1986).
[16] R. Mecke, Z. Elektrochem. **54**, 38 (1950), and references therein.
[17] A. Amrein, H. R. Dübal, M. Lewerenz, and M. Quack, Chem. Phys. Lett. **112**, 387 (1984).

[18]M. Lewerenz and M. Quack, Chem. Phys. Lett. **123**, 197 (1986).
[19]J. S. Wong, Thesis, Berkeley, 1981; J. S. Wong and C. B. Moore, in *Proceedings of the 28th Congress International Union Pure Applied Chemistry Congress, Vancouver, 1981*, edited by K. J. Laidler, p. 353; J. Chem. Phys. **77**, 603 (1982).
[20]A. Campargue and F. Stoeckel, J. Chem. Phys. **85**, 1220 (1986).
[21]S. F. Fischer, W. Kaiser, and R. Zygan-Maus, in *Energy Storage and Redistribution in Molecules*, edited by J. Hinze (Plenum, New York, 1983), p. 513.
[22]H. R. Dübal, M. Lewerenz, and M. Quack, J. Chem. Phys. **85**, 34 (1986).
[23]M.-C. Chuang, J. E. Baggott, D. W. Chandler, E. W. Farneth, and R. N. Zare, Faraday Discuss. Chem. Soc. **75**, 301 (1983).
[24]D. W. Chandler, W. E. Farneth, and R. N. Zare, J. Chem. Phys. **77**, 4447 (1982).
[25]K. V. Reddy, D. F. Heller, and M. J. Berry, J. Chem. Phys. **76**, 2814 (1982).
[26]H. R. Dübal, M. Lewerenz, and M. Quack (to be published).
[27]G. Graner and G. Guelachvili, J. Mol. Spectrosc. **107**, 215 (1984).
[28]H. R. Dübal and M. Quack (unpublished results); A. Amsein, M. Quack, and U. Schmitt, Mol. Phys. (in press).
[29]G. Herzberg, *Molecular Spectra and Molecular Structure* (Van Nostrand, Toronto, 1945, 1965), Vols. II, III.
[30]J. M. Hollas, *High Resolution Spectroscopy* (Butterworths, London, 1982).
[31]S. Sofue, K. Kawaguchi, E. Hirota, and T. Fujiyama, Bull. Chem. Soc. Jpn. **54**, 897 (1981).
[32]A. Ruoff, H. Bürger, and S. Biedermann, Spectrochim. Acta Part A **27**, 1359 (1971).
[33]N. J. Fyke, P. Lockett, J. K. Thompson, and P. M. Wilt, J. Mol. Spectrosc. **58**, 87 (1975).
[34]T. E. Sullivan and L. Frenkel, J. Mol. Spectrosc. **39**, 185 (1971).
[35]W. L. Meerts and I. Ozier, J. Chem. Phys. **75**, 596 (1981).
[36]A. R. H. Cole, *Tables of Wavenumbers* (Pergamon, Oxford, 1977).
[37]H. Bürger, K. Burczyk, H. Hollenstein, and M. Quack, Mol. Phys. **55**, 255 (1985).
[38]M. Lewerenz and M. Quack (to be published).
[39]R. W. Kirk and P. M. Wilt, J. Mol. Spectrosc. **58**, 102 (1975).
[40]J. P. Champion and G. Graner, Mol. Phys. **58**, 475 (1986).
[41]G. Graner, R. Anttila, and J. Kauppinen, Mol. Phys. **38**, 103 (1979).
[42]M. Quack and J. Troe, Ber. Bunsenges. Phys. Chem. **78**, 240 (1974).
[43]M. Quack, Mol. Phys. **34**, 477 (1977).
[44]M. Quack, J. Chem. Phys. **82**, 3277 (1985).
[45]A. Sinha and J. L. Kinsey, J. Chem. Phys. **80**, 2029 (1984).
[46]S. M. Lederman and R. A. Marcus, J. Chem. Phys. **81**, 5601 (1984).
[47]R. E. Smalley, L. Wharton, and D. H. Levy, Acc. Chem. Res. **10**, 139 (1977).
[48]H. R. Dübal, M. Quack, and U. Schmitt, Chimia **38**, 438 (1984).
[49]C. Douketis, D. Anex, G. Ewing, and J. P. Reilly, J. Phys. Chem. **89**, 4173 (1985).
[50]T. Ha, M. Lewerenz, and M. Quack (in preparation).
[51]J. E. Baggott, H. J. Clase, and I. M. Mills, Spectrochim. Acta Part A **42**, 319 (1986).
[52]J. E. Baggot, D. W. Law, D. P. Lightfoot, and I. M. Mills, J. Chem. Phys. **85**, 5414 (1986).
[53]A. Hoy and I. M. Mills, J. Mol. Spectrosc. **46**, 333 (1973).
[54]G. Graner and H. Bürger, J. Mol. Spectrosc. **115**, 393 (1986).